Journal of Power Sources 181 (2008) 62–68

Contents lists available at ScienceDirect

Journal of Power Sources

journal homepage: www.elsevier.com/locate/jpowsour

Effect of Bi_2O_3 content on characteristics of Bi_2O_3–GDC systems for direct methane oxidation

Ta-Jen Huang*, Jia-Fu Li

Department of Chemical Engineering, National Tsing Hua University, Hsinchu 300, Taiwan, ROC

ARTICLE INFO

Article history:
Received 14 January 2008
Received in revised form 18 March 2008
Accepted 18 March 2008
Available online 25 March 2008

Keywords:
Bismuth oxide
Gadolinia-doped ceria
Temperature-programmed reduction
Methane
Oxidation
De-coking

ABSTRACT

Ceramic systems of Bi_2O_3 and gadolinia-doped ceria (GDC) solid mixture were prepared as catalysts for direct methane oxidation. These systems were characterized by temperature-programmed reduction using hydrogen and carbon monoxide, temperature-programmed reaction of methane, fixed-temperature direct methane oxidation, and X-ray diffraction analysis. Adding Bi_2O_3 to GDC promotes both hydrogen and CO oxidation activities, because of the presence of surface Bi_2O_3 and the high content of mobile oxygen in Bi_2O_3. The reactivity of CO with surface lattice oxygen is enhanced to a higher extent than that of H_2, and this enhanced extent shows a maximum in Bi_2O_3 content. Such a maximum also exists for the catalytic activity of direct methane oxidation. A synergistic effect occurs due to a combination of the high methane reactivity of GDC and the high content of mobile oxygen in Bi_2O_3. The CO_2 selectivity of direct methane oxidation can be modulated by varying the Bi_2O_3 content. The mixing of Bi_2O_3 with GDC also increases the self-de-coking capability of the catalyst during direct methane oxidation, which stabilizes the activity.

1. Introduction

Bismuth oxide (Bi_2O_3) exhibits high oxygen-ion conductivity and has been proposed as an electrolyte material for use in solid oxide fuel cells (SOFCs) [1]. Additionally, Bi_2O_3 has extensive applications as a catalyst for industrial oxidation reactions [2]. However, at low oxygen partial pressures, such as on the anode side of SOFC, pure bismuth oxide is unstable. Moreover, although the high-temperature cubic phase, δ-Bi_2O_3, is one of the most effective oxygen-ion conductors, it is stable only between about 730 °C and its melting point, 824 °C [3]. Therefore, various ceramic systems of bismuth oxide have been proposed to stabilize its δ-phase and exhibit enhanced oxidation activities [4,5]. For methane reactions, doped Bi_2O_3 has been studied as a catalyst of oxidative coupling of methane [6,7].

A novel ceramic system of Bi_2O_3 and gadolinia-doped ceria (GDC) solid mixture has been proposed for direct methane oxidation—the reaction of methane with the lattice oxygen of the catalyst in the absence of gas-phase oxygen; such a Bi_2O_3–GDC system can promote the catalytic activity for direct methane oxidation and eliminate possible carbon deposition [8]. Notably, in direct methane oxidation over the anode in SOFCs, oxygen can be supplied from the cathode-side gas phase through the oxygen-ion conducting electrolyte.

GDC has been adopted as the electrolyte in intermediate-temperature SOFCs [9,10]. It has also been used as the anode cermet material in a direct-methane SOFC [11]. In direct-methane SOFCs [12,13], the activities of methane oxidation to form CO_2 and/or CO influence the fuel efficiency for generating electricity. This is because the electrochemical formation of CO_2 involves four electrons, while that of CO involves only two electrons, with each oxygen ion carrying two electrons; consequently, the current density associated with CO_2 formation is double that associated with CO formation. However, when a direct-methane SOFC is employed in the cogeneration of syngas, the formation of CO but not of CO_2 is preferred.

In direct-methane SOFCs, higher methane oxidation activity is associated with a higher rate of methane decomposition, since methane decomposition is the major step in the methane reaction in the absence of gas-phase oxygen [14]. Methane decomposition yields deposited carbon species, which may accumulate to form coke and deactivate the catalyst. However, the deposited carbon can be removed by gasification with steam [15] or carbon dioxide [16]. Recently, Huang et al. [14,17,18] demonstrated that doped ceria may have a self-de-coking capability, which is the removal of deposited carbon species via gasification by the O species that are supplemented from the bulk lattice of the doped ceria. Notably, "self-de-coking" refers to the removal of carbon in the absence

* Corresponding author. Tel.: +886 3 5716260; fax: +886 3 5715408.
E-mail address: tjhuang@che.nthu.edu.tw (T.-J. Huang).

0378-7753/$ – see front matter © 2008 Elsevier B.V. All rights reserved.
doi:10.1016/j.jpowsour.2008.03.038

of gaseous oxygen. Notably, also, the removal of deposited carbon species increases the rate of methane decomposition and therefore that of methane oxidation.

During SOFC operation, electrical current is generated upon the removal of deposited carbon species by the oxygen species that come from the cathode via the bulk lattice of electrolyte, such that deposited carbon is utilized as the fuel for SOFC [19,20]. In fact, one carbon SOFC design has been proposed to store and utilize the deposited carbon [21]. Therefore, self-de-coking in direct-methane SOFC leads to higher electrical current by increasing the rate of direct methane oxidation [22]. A higher concentration of bulk lattice oxygen reportedly results in higher self-de-coking capability [14], which may solve the problem of coking in direct methane oxidation and increase methane conversion.

The high oxygen-ion conductivity of Bi_2O_3 is associated with its high concentration of oxygen vacancies to contain bulk lattice oxygen [23]. This bulk lattice oxygen is highly mobile and can be used to promote the total oxidation of the deposited carbon species [8]. Restated, Bi_2O_3 has a high content of mobile oxygen [1], which can be utilized to increase the rate of direct methane oxidation. Therefore, when Bi_2O_3 is mixed with GDC, the high concentration of bulk lattice oxygen in Bi_2O_3 should promote the self-de-coking capability of this ceramic system. Accordingly, when this Bi_2O_3–GDC system is used to catalyze direct methane oxidation, the coking problem can be reduced or even eliminated [8].

In this work, various Bi_2O_3–GDC systems were prepared as catalysts of direct methane oxidation in an attempt to take advantage of the high concentration of usable lattice oxygen in Bi_2O_3. Methane oxidation activity and the associated CO and hydrogen oxidation activities increased with the addition of Bi_2O_3 to GDC and a synergistic effect was observed. An optimal Bi_2O_3 content in the Bi_2O_3–GDC system for direct methane oxidation was demonstrated to exist.

2. Experimental

2.1. Preparation of GDC and Bi_2O_3–GDC system

GDC was prepared by co-precipitation. The details of the method have been described elsewhere [17]. Suitable amounts of gadolinium nitrate and cerium nitrate were used to yield a nominal atomic ratio of Gd:Ce = 1:9. The GDC powders were calcined by heating in air at a rate of 10 °C min^{-1} to 800 °C and held for 4 h before cooling. The GDC prepared in this work was $(GdO_{1.5})_{0.1}(CeO_2)_{0.9}$.

The Bi_2O_3–GDC system was prepared by mixing GDC and Bi_2O_3 powders with the designated weight ratio. Then, the solid mixture was calcined at 800 °C for 4 h to yield the Bi_2O_3–GDC system. All tests were performed on calcined samples without pre-reduction.

2.2. Temperature-programmed reduction using H_2 and CO

Temperature-programmed reduction using hydrogen (H_2-TPR) and temperature-programmed reduction using carbon monoxide (CO-TPR) were performed at atmospheric pressure in a continuous flow reactor charged with 50 and 100 mg of sample catalyst, respectively. The charge was fixed by quartz wool and quartz sand downstream of the bed. The reactor was made of an 8-mm i.d. quartz U-tube that was embedded in an insulated electric furnace. A K-type thermocouple was inserted into the catalyst bed to measure and control the bed temperature.

H_2-TPR tests were performed with 10% H_2 in Ar at a flow rate of 30 ml min^{-1}, heated from room temperature to the designated temperature at a rate of 10 °C min^{-1}; the material was then held at that temperature for the designated time before cooling. Some details of the H_2-TPR test have been presented elsewhere [18]. CO-TPR tests were performed using the same temperature program but with 1% CO in Ar at 20 ml min^{-1}.

2.3. Temperature-programmed reaction of methane

The test of temperature-programmed reaction of methane (CH_4-TPR_x) was conducted using the same reactor setup as was used for the TPR tests; the reactor was also charged with 100 mg of sample catalyst. The gas feed was passed through an oxygen filter to eliminate trace amounts of oxygen. A blank test was performed and the results indicated that no oxygen leak occurred in this reactor system.

A mixture of 1% CH_4 in argon was fed to the catalyst bed at a flow rate of 20 ml min^{-1}. The CH_4-TPR_x test began from room temperature and continued to the designated temperature at a rate of 10 °C min^{-1}; the material was then held at that temperature for 1 h before cooling. The reactor outflow was analyzed on-line by gas chromatography (China Chromatograph 8900, Taiwan), CO-NDIR (non-dispersive infrared, Beckman 880), and CO_2-NDIR (Beckman 880).

2.4. Fixed-temperature reaction of methane

The fixed-temperature test was performed in the same reactor setup as the CH_4-TPR_x test, using 100 mg of sample catalyst. The catalyst was heated to 780 °C in argon. Then, a mixture of 25% CH_4 in argon was fed to the catalyst bed at a flow rate of 100 ml min^{-1} to perform the activity test of methane reaction at 780 °C. The reactor outflow was analyzed using the same detectors as those used in the CH_4-TPR_x test.

3. Results and discussion

3.1. Characteristics of Bi_2O_3–GDC systems

The characteristics of various Bi_2O_3–GDC systems were analyzed using H_2-TPR, X-ray diffraction (XRD) and CO-TPR. Fig. 1 shows that, with the addition of 10 wt% Bi_2O_3 to GDC, the lower-temperature H_2-TPR peak moves from 500 °C for GDC to 278 °C for the Bi_2O_3–GDC system; however, the higher-temperature peak of Bi_2O_3–GDC is at about the same temperature as that of GDC. Notably, the lower-temperature H_2-TPR peak of GDC is considered to be associated with the reduction of the surface capping oxygen (the surface oxygen species) [24,25]. On the other hand, the higher-temperature H_2-TPR peak is considered to be associated with the reduction of the bulk lattice oxygen [18].

As the Bi_2O_3 concentration in the Bi_2O_3–GDC system increases to 25%, an additional H_2-TPR peak appears at 424 °C. The appearance of this additional peak is due to Bi_2O_3 addition and thus can only be attributed to Bi_2O_3. Notably, this Bi_2O_3–GDC system with 25 wt% Bi_2O_3 is a two-phase mixture based on the report of Gil et al. [26], who found that the solubility limit of Bi_2O_3 in the GDC structure was about 0.8 wt%; according to literature ceramic terminology, this two-phase mixture of Bi_2O_3–GDC has been termed Bi_2O_3–GDC system [8]. Therefore, this additional peak may be due to surface Bi_2O_3 particles. A comparison of the XRD spectra shows that an additional XRD peak, such as the one at 27.8°, appears only for 25 wt% Bi_2O_3–GDC and Bi_2O_3–GDC with higher Bi_2O_3 content, as shown in Fig. 2. Additionally, Fig. 3 shows the image of energy dispersive X-ray (EDX) analysis over a 600 °C-reduced 40 wt% Bi_2O_3–GDC sample. The composition of the surface "spectrum 32" (as designated in Fig. 3) particle was 84.66 at.% Bi and 14.64 at.% O with trace amount of Ce and Gd. This indicates the presence of segregated surface particles that are composed of a large amount of elemental Bi and a relatively small amount of ele-

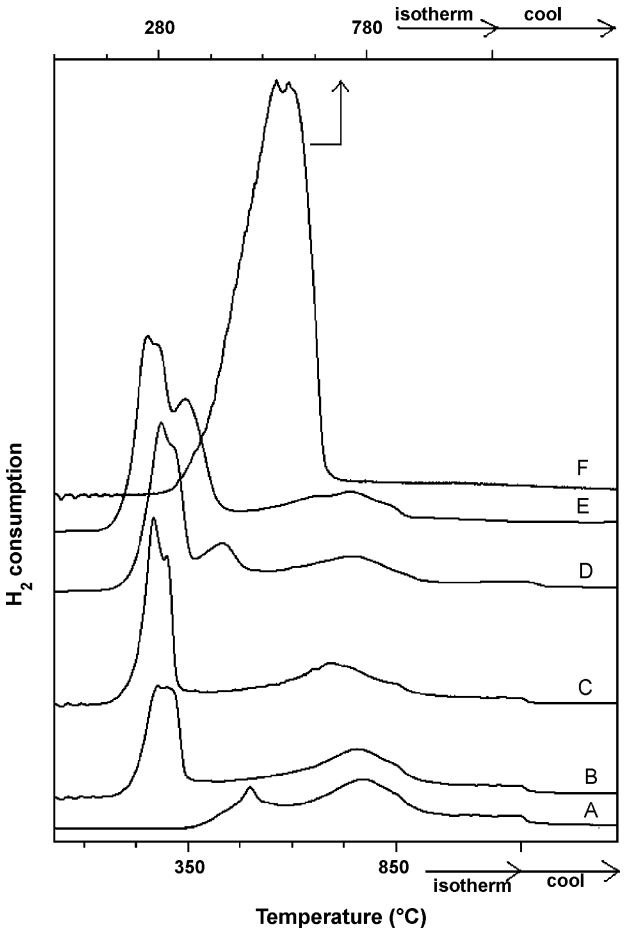

Fig. 1. H_2-TPR profiles of various Bi_2O_3–GDC systems. (A) GDC; (B) 10 wt% Bi_2O_3–GDC; (C) 20 wt% Bi_2O_3–GDC; (D) 25 wt% Bi_2O_3–GDC; (E) 40 wt% Bi_2O_3–GDC; (F) Bi_2O_3. Samples A–E were temperature-programmed to 850 °C while F was programmed only to 780 °C due to the melting point of Bi_2O_3 at 824 °C.

mental O. Notably, these surface particles should have been formed before the Bi_2O_3 content in the Bi_2O_3–GDC system increases to 25%. Notably, also, due to the limitation of XRD analysis, such particles can be too small to be detected by XRD. However, these surface particles, no matter how small, can have an effect on the surface activity. Additionally, in these surface particles, the above compo-

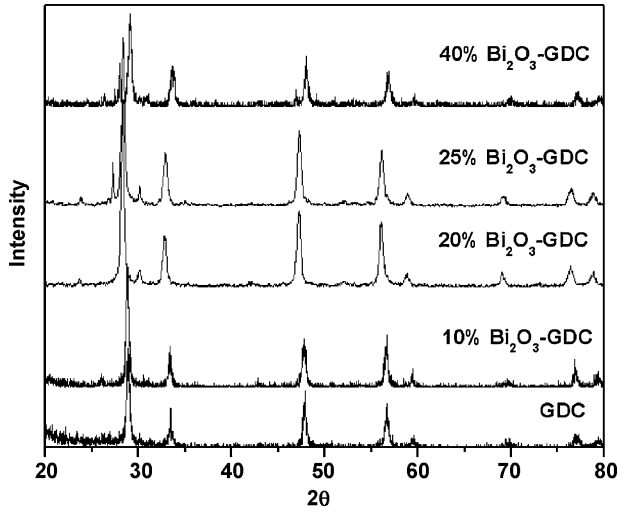

Fig. 2. XRD diagrams of various Bi_2O_3–GDC systems.

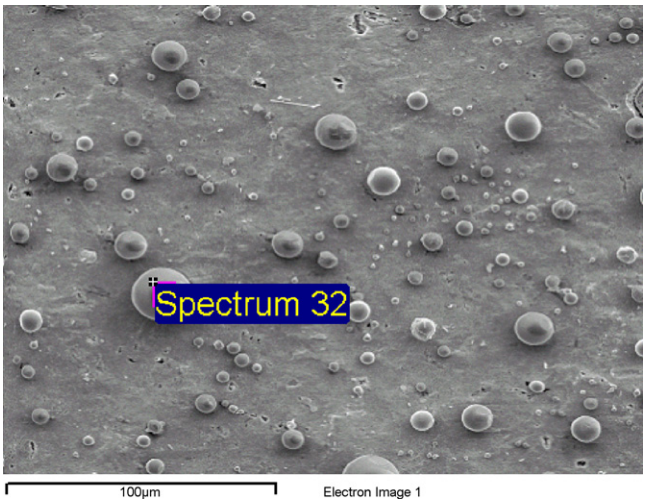

Fig. 3. EDX image over a 600 °C-reduced 40 wt% Bi_2O_3–GDC sample.

sition data indicate that the elemental O is associated mostly with the elemental Bi and GDC accounts only trace amount.

Table 1 presents the total H_2-TPR peak area, representing the total amount of H_2 consumed during H_2-TPR. H_2 consumption increases with amount of added Bi_2O_3, because of the high content of mobile oxygen in Bi_2O_3 [1]. Notably, the H_2 consumed during H_2-TPR is oxidized by the oxygen species in the catalyst and the H_2 consumption is thus equivalent to that of the lattice oxygen of the catalyst. The results in Table 1 show that almost all of O in Bi_2O_3 was consumed and so Bi_2O_3 should have been reduced to Bi metal at the end of the test. The peak temperature of Bi_2O_3, about 560 °C, as shown in Fig. 1, also indicates that Bi_2O_3 can be completely reduced at 780 °C in the H_2-TPR test. Therefore, all of O in Bi_2O_3 can be extracted from the bulk to the surface for oxidation.

Fig. 1 also shows that the extraction of lattice oxygen species in Bi_2O_3 for H_2 oxidation occurs at a much higher temperature than that in Bi_2O_3–GDC systems. Therefore, the reactivity of H_2 with the surface lattice oxygen of Bi_2O_3 is lower than that of Bi_2O_3–GDC. Since the H_2 reactivity of Bi_2O_3–GDC is also higher than that of GDC, the high H_2 reactivity of the Bi_2O_3–GDC systems, as revealed by the low H_2-TPR peak temperature, may be considered to be due to a synergistic effect between Bi_2O_3 and GDC. This synergistic effect involves a combination of the surface Bi_2O_3 particles and the high content of mobile oxygen in Bi_2O_3. Notably, the amount of mobile or active oxygen species in Bi_2O_3–GDC is less than that in Bi_2O_3, as revealed by the total amount of H_2 consumption in Table 1. This is because, although GDC has high O content than Bi_2O_3, as also shown in Table 1, the amount of mobile or active oxygen species in GDC for oxidation is much less than that in Bi_2O_3. Notably, also, the amount of H_2 consumption is equivalent to that of oxygen consumption according to the reaction of hydrogen oxidation: $H_2 + O \rightarrow H_2O$. Notably, also, a higher rate of H_2 oxidation corresponds to a larger amount of H_2 consumption. Therefore, adding Bi_2O_3 to GDC increases the amount of mobile or active oxygen species in this system, increasing the H_2 oxidation rate, such that the total amount of H_2 consumption during H_2-TPR increases with Bi_2O_3 content, as revealed in Table 1.

Fig. 4 displays the CO-TPR profiles. The peak temperature of Bi_2O_3–GDC is much lower than that of pure Bi_2O_3. These low-temperature peaks are also much larger than the low-temperature peak of pure GDC. This difference is also considered to be associated with a synergistic effect between Bi_2O_3 and GDC. Notably, a lower CO-TPR peak temperature also indicates a higher CO reactivity with the surface lattice oxygen of the catalyst; on the other

Table 1
Total peak areas of H_2-TPR and CO-TPR profiles[a] of various Bi_2O_3–GDC systems

	Total H_2 consumption during H_2-TPR (10^3 μmol g^{-1})	Total CO_2 formation during CO-TPR (10^3 μmol g^{-1})	Ratio of CO-TPR to H_2-TPR[d]
GDC[b]	1.49	2.12	1.42
10 wt% Bi_2O_3–GDC	2.42	3.38	1.40
20 wt% Bi_2O_3–GDC	2.34	4.14	1.77
25 wt% Bi_2O_3–GDC	2.87	4.68	1.63
40 wt% Bi_2O_3–GDC	4.06	5.56	1.37
Bi_2O_3[c]	8.11	8.27	1.02

[a] GDC and Bi_2O_3–GDC were temperature-programmed to 850 °C while pure Bi_2O_3 was programmed only to 780 °C due to the melting point of Bi_2O_3 at 824 °C.
[b] The total O content in GDC, i.e. $(GdO_{1.5})_{0.1}(CeO_2)_{0.9}$, is 11270 μmol g^{-1} GDC.
[c] Since one-fourth of the oxygen sites are vacant in the fluorite-type lattice [1], calcined bismuth oxide is Bi_4O_8, which has an O content of 8299 μmol g^{-1}.
[d] Obtained by dividing the total CO_2 formation during CO-TPR by the total H_2 consumption during H_2-TPR.

hand, a larger peak area indicates a larger amount of the reactant, e.g. oxygen species in the situation of this work, which is available at the designated peak temperature; therefore, higher reactivity and larger reactant amount are two separate issues. Notably, also, only the surface oxygen can directly attend the reaction and the bulk lattice oxygen has to be transported to the surface for reaction. As also shown in Fig. 4, the total CO-TPR peak area over Bi_2O_3, corresponding to the total amount of CO_2 formed during CO-TPR over Bi_2O_3, is much higher than that over GDC. Therefore, the total amount of CO_2 formed during CO-TPR increases with Bi_2O_3 content, as revealed in Table 1. This fact is also considered to follow from the high content of mobile oxygen in Bi_2O_3.

Table 1 also indicates that, although the total oxygen consumption during either H_2-TPR or CO-TPR increases with the addition of Bi_2O_3 to GDC, the consumption of oxygen during CO-TPR is always higher than that during H_2-TPR. Notably, both H_2 consumption and CO_2 formation during TPR analyses are equivalent to oxygen consumption; CO_2 formation during CO-TPR is via CO oxidation by the oxygen species in the catalyst: $CO + O \rightarrow CO_2$. Since the consumptions of oxygen from Bi_2O_3 during H_2-TPR and CO-TPR are about equal, the higher oxygen consumption of Bi_2O_3–GDC should be attributed to GDC. Dividing the total amount of CO_2 formed during CO-TPR by that of H_2 consumed during H_2-TPR yields a ratio for GDC that markedly exceeds that for Bi_2O_3, as indicated in Table 1. Notably, this ratio shows a comparison of the overall reactivity of CO oxidation to that of H_2 oxidation. This indicates that the reactivity of CO with the surface lattice oxygen is higher than that of hydrogen, because the surface OH species formed by H_2 oxidation can have an inhibition effect on the reactivity [17]. Additionally, this ratio reaches a maximum at about 20 wt% Bi_2O_3.

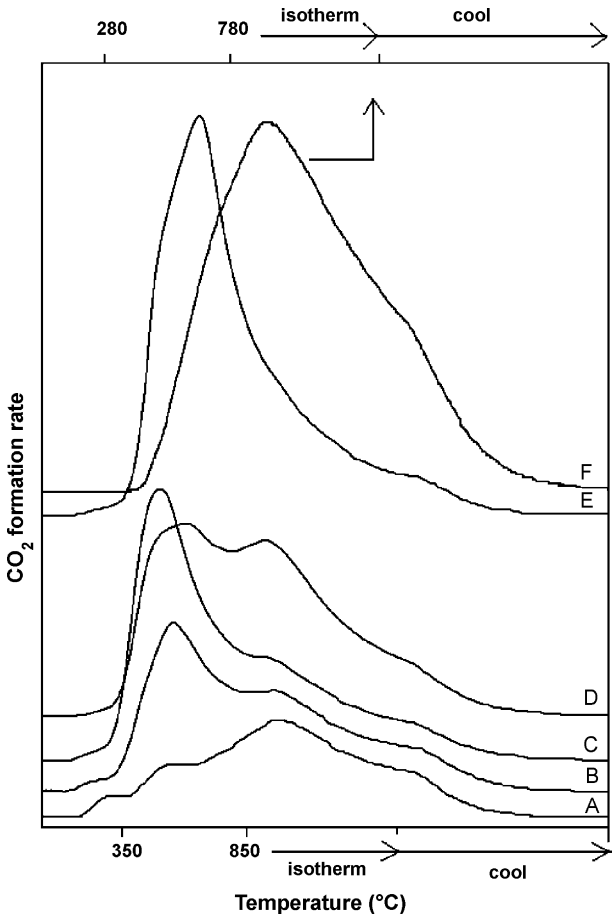

Fig. 4. CO-TPR profiles of various Bi_2O_3–GDC systems. The samples and the test designations are as in Fig. 1.

The above results show that the addition of Bi_2O_3 to GDC enhances both the H_2 and CO oxidation activities of the catalyst, because of the presence of surface Bi_2O_3 and the high content of mobile oxygen in Bi_2O_3. A synergistic effect between Bi_2O_3 and GDC is evident not only in hydrogen oxidation but also in CO oxidation. The reactivity of CO with the surface lattice oxygen is enhanced to a higher extent than that of hydrogen; this enhanced extent shows a maximum in Bi_2O_3 content.

3.2. *Effect of Bi_2O_3 content on activity of direct methane oxidation*

The activities of direct methane oxidation over various Bi_2O_3–GDC systems were characterized by CH_4-TPR$_x$ in the absence of gas-phase oxygen. Fig. 5(a) and (b) shows the CH_4-TPR$_x$ results for GDC and pure Bi_2O_3, respectively. The activity of methane oxidation over GDC, in terms of the total amount of carbon oxides formed, is much higher than that over pure Bi_2O_3. The low methane activity of Bi_2O_3 is considered to follow from the low affinity between CH_4 and Bi_2O_3 or Bi. Notably, during CH_4-TPR$_x$, Bi_2O_3 is reduced to the Bi metal. A comparison between Fig. 5(a) and (b) indicates that the rate of CO_2 formation over GDC becomes appreciable at about 150 °C and that over Bi_2O_3 becomes appreciable at about 300 °C. Over Bi_2O_3 and from 200 to 300 °C, the rate of CO_2 formation is roughly constant at a very low level when some Bi metal may have been formed over the Bi_2O_3 surface. Additionally, the lower peak associated with CO_2 formation over GDC is at 280 °C, which is much lower than that over Bi_2O_3 at 560 °C, indicating that the reactivity of methane over Bi–Bi_2O_3 can be very much lower than that over GDC. Restated, the formation of Bi metal does not yield a methane oxidation activity that is higher than that over GDC. Notably, the peak temperature of Bi_2O_3 at 560 °C during CH_4-TPR$_x$ equals that during H_2-TPR, indicating that the Bi metal should have been formed in large amount. Notably, also, direct methane oxidation by the lattice oxygen may proceed to produce CO and hydrogen [19]: $CH_4 + O \rightarrow CO + 2H_2$.

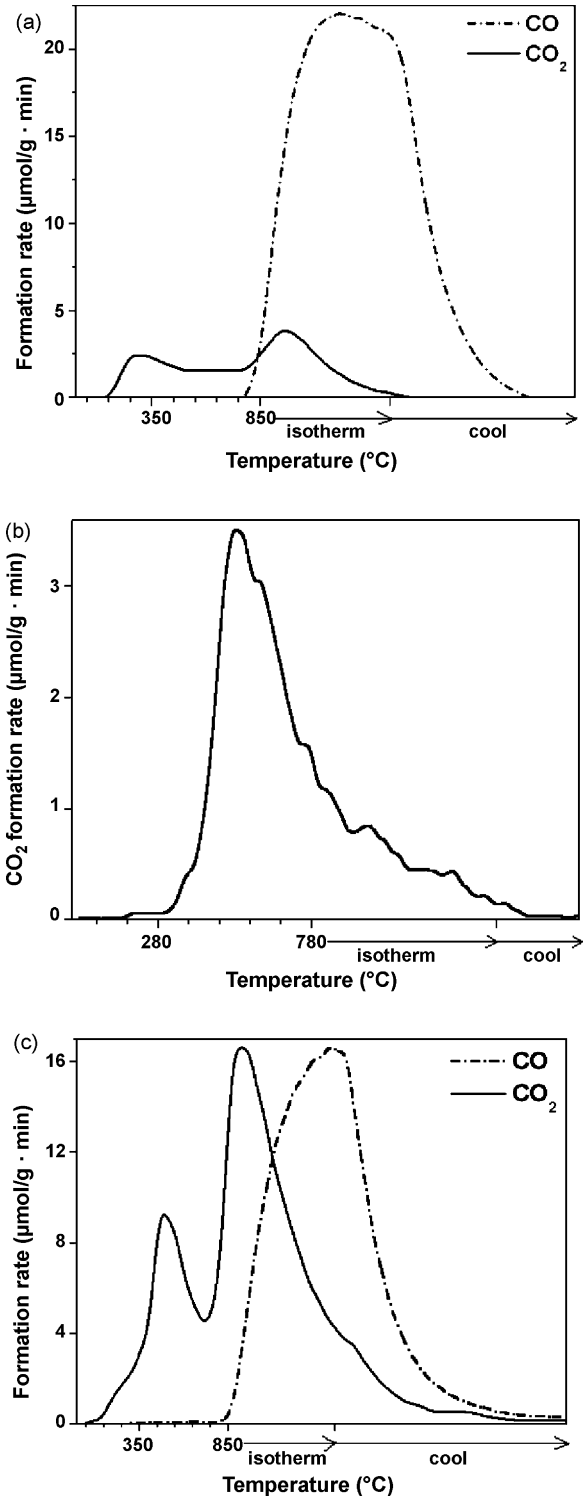

Fig. 5. CH_4-TPR_x profiles: (a) GDC, (b) Bi_2O_3 and (c) 25% Bi_2O_3–GDC.

Fig. 5(a) and (b) also shows that the carbon oxide species formed over GDC is mostly CO while that over Bi_2O_3 is completely CO_2. This is because Bi_2O_3 has a much higher content of mobile oxygen and thus a higher concentration of surface oxygen species, which enhances CO_2 formation [22,27], especially when the high content of mobile oxygen in Bi_2O_3 is associated with its low methane oxidation activity. Thus, the surface Bi enrichment over Bi_2O_3–GDC can increase the CO_2 selectivity, as shown in Table 2. Additionally,

Table 2
Amounts of carbon oxides and CO_2 formation and CO_2 selectivity during CH_4-TPR_x tests over various Bi_2O_3–GDC systems

	Total amount of carbon oxides[a] formation (10^3 μmol g^{-1})	Amount of CO_2 formation (10^3 μmol g^{-1})	CO_2 selectivity[b]
GDC	1.74	0.273	0.157
10% Bi_2O_3–GDC	1.85	0.495	0.268
20% Bi_2O_3–GDC	2.19	0.768	0.351
25% Bi_2O_3–GDC	2.31	1.13	0.489
40% Bi_2O_3–GDC	2.08	1.28	0.615
70% Bi_2O_3–GDC	1.75	1.63	0.931
Bi_2O_3	0.132	0.132	1

[a] Carbon oxides include CO and CO_2.
[b] CO_2 selectivity = amount of CO_2/amount of CO + amount of CO_2.

Fig. 5(a) shows that the rate of CO formation over GDC becomes significant at about 780 °C, which is the temperature at which the bulk lattice oxygen of GDC to become highly mobile [27]. This indicates that CO formation is associated with the bulk lattice oxygen species of GDC when these oxygen species become highly mobile, in agreement with the report of Huang and Wang [27].

A comparison of Fig. 5(a) and (c) indicates that, with the addition of 25 wt% Bi_2O_3 to GDC, the formed solid mixture system exhibits a dramatically increased CO_2 formation rate; however, the CO formation rate over Bi_2O_3–GDC is less than that over GDC. Nevertheless, the drop in the CO formation rate is smaller than the increase in the CO_2 formation rate, as also shown in Fig. 6(a) and (b). Since CH_4 oxidation produces CO_2 and/or CO, the total amounts of carbon oxides, CO and CO_2, formed is related to methane conversion: $\Delta CH_4 = \Delta CO + \Delta CO_2$ based on carbon balance. Notably, possible carbon deposition over the catalyst was analyzed following the CH_4-TPR_x tests and found to be negligible. Therefore, the larger increase in the rate of CO_2 formation and the associated smaller decrease in the rate of CO formation lead to the formation of more carbon oxides and thus higher methane activity. However, the methane activity of Bi_2O_3 is relatively low and so the methane activity of Bi_2O_3–GDC should drop as the Bi_2O_3 content increases over a certain threshold as it is added to GDC and a maximum should be reached. Table 2 indicates that this maximum is at about 25 wt% Bi_2O_3. Notably, also, the rate of CO_2 formation declines at a Bi_2O_3 content of around 70–100 wt% Bi_2O_3, reaching finally a very low level over pure Bi_2O_3. This is because insufficient GDC is present over the surface to adsorb methane and thus take advantage of the high oxygen-ion conductivity and the high oxygen content of Bi_2O_3.

A comparison of Tables 1 and 2 reveals that the variation in methane oxidation activity, in terms of carbon oxides formation, is similar to that of the ratio of CO-TPR to H_2-TPR. This may be because the interaction of CH_4 with the surface active site is similar to that of CO, possibly via the C interaction. This interaction can be modulated by varying the Bi_2O_3 content in the Bi_2O_3–GDC system and thus the activity reaches a maximum in a particular Bi_2O_3 content.

The BET areas of GDC, 25 wt% Bi_2O_3–GDC and Bi_2O_3 were determined to be 58, 47 and 38 $m^2\ g^{-1}$, respectively. Thus, the much higher methane oxidation activity over 25 wt% Bi_2O_3–GDC is not associated with a higher surface area. Therefore, the above-observed synergistic effect on the Bi_2O_3–GDC system should be associated with a combination of the high methane reactivity of GDC and the high content of mobile oxygen of Bi_2O_3. The methane oxidation activity increases as Bi_2O_3 is added to GDC because of this synergistic effect. On the other hand, although the Bi species can be present at the surface to promote the supply of the oxygen species for direct methane oxidation, a larger amount of surface Bi species is associated with a lower amount of surface GDC, so the methane oxidation activity is low because of the relatively low methane reac-

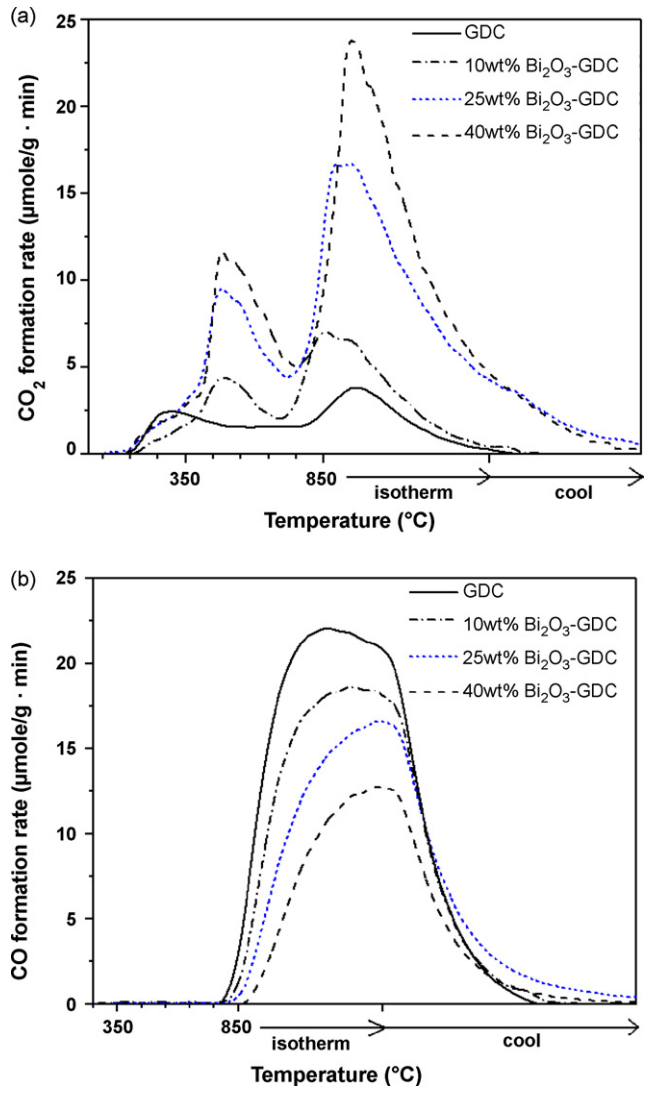

Fig. 6. CH_4-TPR_x profiles of various Bi_2O_3–GDC systems: (a) CO_2 formation and (b) CO formation.

tivity of the Bi species, Bi_2O_3 or the Bi metal, as indicated above. Therefore, the methane reactivity and the oxygen supply ability should come to balance with an intermediate Bi_2O_3 content, verifying the existence of a maximum in methane oxidation activity.

Table 2 also indicates that both the amount of CO_2 formation and the CO_2 selectivity increase with Bi_2O_3 content, because of the high content of mobile oxygen in Bi_2O_3. The extent of the increase in CO_2 formation is much higher than that of methane oxidation activity, as determined by the amount of carbon oxides formed. Therefore, adding Bi_2O_3 to GDC can increase both CO_2 selectivity and methane oxidation activity until a Bi_2O_3 content of about 25% is reached. The above results demonstrate that the CO_2 selectivity of the Bi_2O_3–GDC system can be modulated by varying the Bi_2O_3 content.

3.3. Fixed-temperature activities for direct methane oxidation

Fixed-temperature tests of the activities of Bi_2O_3–GDC systems for direct methane oxidation at 780 °C were performed to verify that the results of the temperature-programmed tests are applicable for isothermal operation; this test temperature was set by considering intermediate-temperature SOFCs and the melting point of Bi_2O_3 at 824 °C. Notably, Bi_2O_3 can be reduced to Bi metal at temperatures of

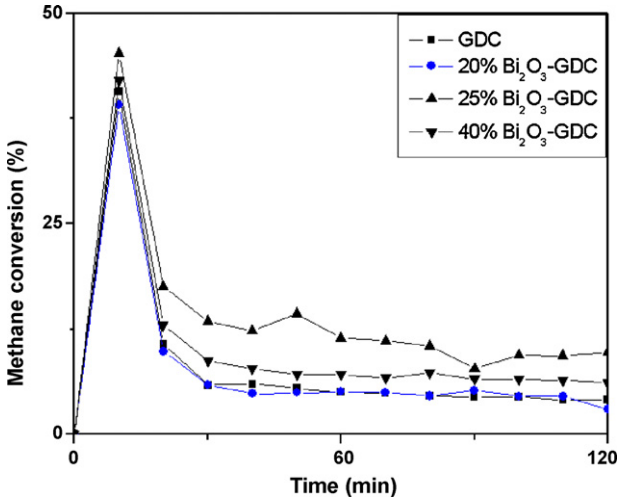

Fig. 7. Fixed-temperature methane conversion profiles of various Bi_2O_3–GDC systems at 780 °C.

over 560 °C, which is the H_2-TPR peak temperature. However, EDX analysis over a 600 °C-reduced Bi_2O_3–GDC sample, as reported in Section 3.1, indicates the association of elemental O with surface Bi element. This suggests that the lattice oxygen of GDC can be supplemented to the surface Bi species to maintain its role as an oxygen storage component. Therefore, the Bi species is adopted to take advantage of the high oxygen-ion conductivity and the high content of mobile oxygen of bismuth oxide.

As shown in Fig. 7, the 25 wt% Bi_2O_3–GDC system has the highest methane activity, which results are consistent with the CH_4-TPR_x results discussed above. The initial jump in the methane activity is considered to be associated with the surface oxygen species over these catalysts without pre-reduction. When the originally existing surface oxygen species are consumed by methane oxidation, the methane oxidation activity becomes quite stable, indicating that any possible coking problem is minimal. This is because the high content of mobile oxygen in Bi_2O_3 enhances the self-de-coking capability. Notably, self-de-coking means the removal of the carbon species produced from methane decomposition and can thus enhance the rate of methane decomposition.

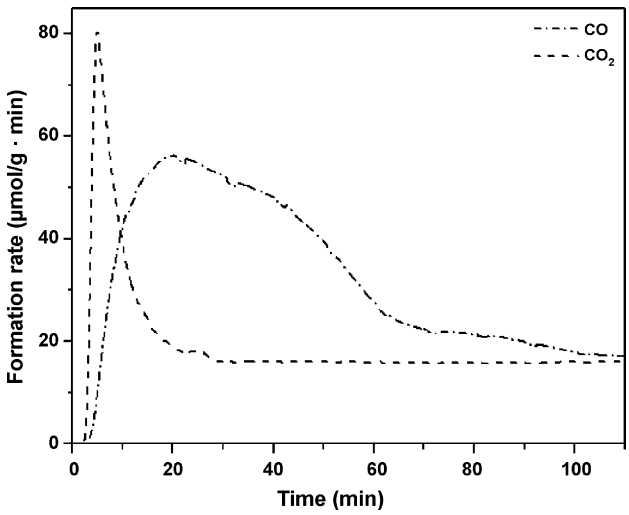

Fig. 8. CO and CO_2 formation profiles of 25 wt% Bi_2O_3–GDC systems during fixed-temperature methane test at 780 °C.

Fig. 8 shows that CO_2 formation rate is constant following an initial jump. This constant CO_2 activity confirms the high capability of self-de-coking of the Bi_2O_3–GDC system. On the other hand, the rate of CO formation also increases drastically initially and then decreases continuously. This drop in the rate of CO formation with time is considered to be due to the continuous drop in the concentration of bulk lattice oxygen as the reaction proceeds. Notably, the oxidation reaction consumes the lattice oxygen in the catalyst and these oxygen species should be replenished from the bulk, which reduces the concentration of bulk lattice oxygen. Notably, also, the rate of CO formation depends on the concentration of the bulk lattice oxygen of GDC [26]. On the other hand, the CO_2 formation rate may be maintained by the presence of surface Bi_2O_3, which acts as an oxygen storage component to promote not only the formation of CO_2 but also the maintaining of the CO_2 formation rate. The constant CO_2 formation rate is regarded as caused by a constant oxygen concentration that is associated with the surface Bi species by quick oxygen replenishment from the bulk, which is enabled by the high oxygen-ion conductivity of Bi_2O_3 at 780 °C [1].

Fig. 8 also shows that an induction period of about 3 min is required for the activation of both CO and CO_2 formation reactions. This induction period follows from the fact that the catalyst is unreduced, since in a test in which the catalyst is prereduced, this induction period disappears. Notably, the unreduced catalyst is activated by the methane gas. Following activation, surface oxygen species in the unreduced catalyst cause the jump in both CO and CO_2 formation rates. Additionally, the formation rate of CO_2 initially exceeds that of CO. Then, the formation rate of CO becomes much higher than that of CO_2. It shows that, during the test period, the amount of CO_2 formed with the 25 wt% Bi_2O_3–GDC catalyst is less than that of CO; this indicates that the CO_2 selectivity is less than one half, in agreement with that shown in Table 2 for the CH_4-TPR_x test. Notably, during SOFC operation, oxygen is supplied continuously from the cathode-side gas phase through the bulk lattice of the oxygen-ion conducting electrolyte; thus, the lattice oxygen concentration of the anode bulk is not overly depleted, although a concentration difference exists [20]. Since the concentration of bulk lattice oxygen affects the formation rate of carbon oxides, the results of a short fixed-temperature test, when the bulk lattice oxygen has not been overly depleted, may be more useful in the simulation of the SOFC anode operation. However, actual SOFC tests with the Bi_2O_3–GDC system as anode material are required to confirm finally the performance of the system in direct methane oxidation in SOFCs.

4. Conclusions

(1) Adding Bi_2O_3 to GDC increases both the hydrogen and the CO oxidation activities of the catalyst, because of the presence of surface Bi_2O_3 and the high content of mobile oxygen in Bi_2O_3.
(2) The reactivity of CO with the surface lattice oxygen is enhanced more than that with hydrogen, and the extent of this enhancement reached a maximum in Bi_2O_3 content. This maximum also exists in the catalytic activities of direct methane oxidation during CH_4-TPR_x and the fixed-temperature reaction of methane.
(3) The Bi_2O_3–GDC system exhibits a synergistic effect, because of a combination of the high methane reactivity of GDC and the high content of mobile oxygen in Bi_2O_3.
(4) The CO_2 selectivity in direct methane oxidation can be modulated by varying the Bi_2O_3 content.
(5) The mixing of Bi_2O_3 with GDC increases the self-de-coking capability of the catalyst during direct methane oxidation, which stabilizes the activity.

References

[1] N.M. Sammes, G.A. Tompsett, H. Nafe, F. Aldinger, J. Eur. Ceram. Soc. 19 (1999) 1801–1826.
[2] R. Irmawati, M.N. Noorfarizan Nasriah, Y.H. Taufiq-Yap, S.B. Abdul Hamid, Catal. Today 93–95 (2004) 701–709.
[3] M. Mehring, Coord. Chem. Rev. 251 (2007) 974–1006.
[4] P. Shuk, H.D. Wiemhofer, U. Guth, W. Gopel, M. Greenblatt, Solid State Ionics 89 (1996) 179–196.
[5] Y. Zeng, Y.S. Lin, J. Catal. 182 (1999) 30–36.
[6] Y. Zeng, Y.S. Lin, Appl. Catal. A: Gen. 159 (1997) 101–117.
[7] Y. Zeng, Y.S. Lin, J. Catal. 193 (2000) 58–64.
[8] T.J. Huang, J.F. Li, J. Power Sources 173 (2007) 959–964.
[9] C. Xia, M. Liu, Solid State Ionics 144 (2001) 249–255.
[10] Y.J. Leng, S.H. Chan, S.P. Jiang, K.A. Khor, Solid State Ionics 170 (2004) 9–15.
[11] A.A. Yaremchenko, A.A. Valente, V.V. Kharton, I.A. Bashmakov, J. Rocha, F.M.B. Marques, Catal. Commun. 4 (2003) 477–483.
[12] J.B. Wang, J.C. Jang, T.J. Huang, J. Power Sources 122 (2003) 122–131.
[13] Y. Lin, Z. Zhan, J. Liu, S.A. Barnett, Solid State Ionics 176 (2005) 1827–1835.
[14] T.J. Huang, C.H. Wang, Chem. Eng. J. 132 (2007) 97–103.
[15] V.R. Choudhary, S. Banerjee, A.M. Rajput, Appl. Catal. A: Gen. 234 (2002) 259–270.
[16] J.B. Wang, Y.S. Wu, T.J. Huang, Appl. Catal. A: Gen. 272 (2004) 289–298.
[17] T.J. Huang, T.C. Yu, Catal. Lett. 102 (2005) 175–181.
[18] T.J. Huang, H.C. Lin, T.C. Yu, Catal. Lett. 105 (2005) 239–247.
[19] T.J. Huang, M.C. Huang, J. Power Sources 168 (2007) 229–235.
[20] T.J. Huang, M.C. Huang, Chem. Eng. J. 135 (2008) 216–223.
[21] M. Ihara, K. Matsuda, H. Sato, C. Yokoyama, Solid State Ionics 175 (2004) 51–54.
[22] T.J. Huang, C.H. Wang, J. Power Sources 163 (2006) 309–315.
[23] N. Jiang, E.D. Wachsman, S.H. Jung, Solid State Ionics 150 (2002) 347–353.
[24] O.A. Marina, M. Mogensen, Appl. Catal. A: Gen. 189 (1999) 117–126.
[25] T.J. Huang, Y.C. Kung, Catal. Lett. 85 (2003) 49–55.
[26] V. Gil, J. Tartaj, C. Moure, P. Duran, J. Eur. Ceram. Soc. 27 (2007) 801–805.
[27] T.J. Huang, C.H. Wang, Catal. Lett. 118 (2007) 103–108.